PROCEEDINGS, 49th Workshop on Geothermal Reservoir Engineering
Stanford University, Stanford, California, February 12-14, 2024
SGP-TR-227

Numerically Testing Conceptual Models of the Utah FORGE Reservoir Using July 2024 Circulation Test Data

Lynn Munday and Robert Podgorney

Idaho National Laboratory, Idaho Falls, ID, USA

Keywords: Utah FORGE, Enhanced Geothermal Systems, MOOSE, FALCON

ABSTRACT

Over the past several years, many new data sets have become available regarding the characterization of the Utah FORGE reservoir. These include, but are not limited to, the stimulation of Well 16A, the drilling and completion of Well 16B, and interwell circulation confirmatory testing. As part of the characterization efforts, conceptual models of the reservoir are re-examined as new data become available. As part of the planning for FORGE activities, numerical models are often used to predict the reservoir response to the planned testing. Stochastic methods are often employed to bound uncertainty and allow for evaluation of comprehensive ranges of key reservoir parameters. For the most recent interwell circulation confirmatory testing (July 2023), a priori numerical model predictions did bound the observed behavior (Xinj et al., 2023), but key deviations from expected behavior prompted the FORGE team to reevaluate our conceptual model of the reservoir.

In early October 2023, key members of the development, testing, and monitoring teams met for 2 days to review newly collected data and discuss 'interesting' or 'key' observations. From these discussions, 15 Key Observations were documented, with several significant ones being that the discrete fracture network developed from the 16A stimulation data may not be appropriate and that the early time pressure data obtained during the summer 2023 reservoir testing were best described using radial solutions.

In July 2023, two campaigns of interwell confirmatory testing were conducted, the first set of tests occurred on July 4-5 and the second set on July 18-19. The second set of circulation tests conducted at the Utah FORGE site between the injection well 16A(78)-32 and production well 16B(78)-32 on July 18 and 19, 2023 are used to calibrate material properties in a thermal-hydraulic-mechanical (THM) simulation of the discrete fracture network connecting the wells. The spatially and temporally varying reservoir properties are calibrated to match the time dependent pressure and production profiles from the circulation tests. In future work, this calibrated model will be coupled to the native state THM model of the FORGE reservoir to predict surface deformation and strains resulting from pumping schedules.

1. INTRODUCTION

The Utah FORGE site is an enhanced geothermal system using existing and created fracture networks in deep crystalline rocks to transfer thermal energy to a working fluid pumped between the injection and production wells. Injection well 16A(78)-32 was completed in December 2020 and has undergone several hydraulic stimulations to increase the fracture network (McLennan et al., 2023). Based on the produced seismic cloud from these stimulations, production well 16B(78)-32 was placed 300 feet above 16A and completed in June 2023. Circulation tests were performed in July 2023 to demonstrate connectivity between the injection well 16A and production well 16B (Xinj et al., 2024). In this paper, we use the FALCON application developed at Idaho National Laboratory (Podgorney et al, 2021) to perform coupled thermal-hydraulic-mechanical finite element simulations of the July circulation tests to examine varying conceptualizations of the fracture and matrix properties, with the goal of matching 16A wellhead pressure and 16B production rate. Our objective is to characterize the stimulated fractures connecting the injection and production wells by parameterizing the porous flow materials properties of the fracture and surrounding matrix.

2. CONCEPTUAL MODEL REEVALUATION

In October 2023, key members of the development, testing, and monitoring teams met for 2 days to review newly collected data and discuss 'interesting' or 'key' observations. Table 1 below summarizes:

Table 1. 1 Topic and data types discussed at the October 2023 meeting.

Topic	Summary
Observations from 16A Drilling and Characterization	Rock types, fractures, key observations
Stimulation of 16A	Pressures, fluids, flow rates and MEQ. Reservation creation key takeaways
16A Flowback geochemistry and tracers	Observation and trends in flowback waters. What do they tell us about the reservoir and fractures?
16A Slug testing	Test description and procedures, observed pressures, flow rates, etc. Reservation permeability characterization key takeaways
Observations from 16B Drilling and Characterization	Rock types, fractures, key observations
16A-16B Interwell Flow Testing	Test description and procedures, observed pressures, flow rates, etc. Reservation connectivity key takeaways

From these discussions, 15 *Key Observations* were documented. Podgorney (2024) discussed the process and evaluation as part the the Utah FORGE Modeling and Simulation Community Forum (https://utahforge.com/numerical-modeling/#m-s-forum). The Key Observations are presented below.

Key Observation documented at the October 2023 conceptual model meeting.

1. From the seismic team: Absolute MEQ locations for stage 1 and 2 – there is large uncertainty. Fitting planes may be an over-interpretation. We cannot say the MEQ data are related to natural fractures with any certainty. **Key Takeaway—The DFN based on the plane-fitting to the MEQ catalog that we have been using for modeling the reservoir has little validity.**
2. From the reservoir engineering team: Effects of various stimulation fluids likely only near 16A. Viscosity is a function of temperature and time @ a given temperature. **Key Takeaway—The far field fluid rheology is likely the same between all stimulations.**
3. From the geology team: >8 tons of saline material removed during flowback from 16A. **Key Takeaway—Likely a significant increase in porosity/permeability near the 16A wellbore, AND fracture filling material is likely dissolvable.**
4. From the hydrogeology testing team: Radial model was best fit for slug tests—volume interrogated likely small. Transmissivity (near wellbore) is quite high….but extent is uncertain. 10's of meters? Not more than 50?. **Key Takeaway—Potentially planar fractures stimulated near the 16A wellbore.**
5. From the geology team: A large portion 16B fractures in tangent section were vertical (FMI says yes (80-90%), core data can't be certain). **Key Takeaway—More analysis needs to be done to confirm this…if true it would indicate that vertical fracturing dominates both the original natural fracture orientations and stimulated fracture orientations.**
6. From the reservoir engineering team: Rate of leakoff/pressure drop after shut in seems "smaller" after larger volume injections, i.e., the formation holds more pressure after higher volume injection events. **Key Takeaway—Larger volume injections essentially "fill" all the available storage (natural fractures?), and the reservoir is effectively isolated and closed.**
7. From the geology team: Zones of high fracture intensity ~align between A and B. Individual fractures (most highly conductive zones on FMI) seem to align vertically. **Key Takeaway—Geologic structure between Wells 16A and 16B has continuity and exact geometric relationship needs to be confirmed.**
8. From the reservoir engineering team: Fracture opening pressure different between OH and perffed zones. This is likely a near wellbore tortuosity artifact. This relates to wellbore pressure. **Key Takeaway—Near wellbore pressure drop is affected/controlled by more than just number of effective perforations.**
9. From the reservoir engineering team: We have separated systems from each stage. **Key Takeaway—Stage 1 and Stage 2 DFN may be inappropriate as the fractures were interconnected, as related to Point 1.**
10. From the geology team: We may have encountered less metamorphic rocks in 16B versus 16A. **Key Takeaway—Practical implications uncertain, may have an effect on mechanical rock properties.**
11. From the geology team: Tracer was found in the cored intervals and correlated to injection locations, and also cross-zone flow in the formation, but not necessarily in the injection well. **Key Takeaway—This may add confidence to DFN (see Point 1), as the hypocenters were used to choose coring intervals.**
12. From the reservoir engineering team: Pressure response time between A & B decreased over the testing campaign. 40 mins, 5 min, 1 min, less. **Key Takeaway—Injections essentially "fill" all the available storage (natural fractures?), and the reservoir is effectively isolated and closed. Fluid filling available storage makes the system more responsive.**
13. From the hydrogeology testing team: Seemingly no changes in permeability over the July 2023 testing campaign. **Key Takeaway—July 2023 injections did not have a permanent effect on the reservoir. Further, the reservoir permeability did not respond in an expected poroelastic way.**
14. From the hydrogeology testing team: Zonation of permeability between A & B. **Key Takeaway—Permeability near Well 16A is significantly higher than the permeability near Well 16B. The nature of the transition is uncertain.**

15. From the seismic team: Fracturing did occur during the July 2023 flow testing, mostly measurable in Stage 3 (cannot comment on other stages). **Key Takeaway—Pressure drop associated with flowing Well 16B was not enough, or the well wasn't connected to the formation enough, to keep the far field pressure below the frack gradient.**

2.1 Simplified Conceptual Models

Geo Energie Suisse developed the simplified conceptual model shown in Figure 1a based on the June 2023 well 16A slug test data. The simplified model summarized above in observation 4 has three main regions: a region of high transmissivity around the injection point of well 16A, a region of low transmissivity around the production point of well 16B and the remainder of the fracture modeled as a radially decreasing transmissivity between 16A and 16B. Several factors could lead to a region of high transmissivity around well 16A including stimulation and opening of existing fractures, washing or dissolving halite out of the fracture network. The low transmissivity around 16B could be due to blockage of the fracture network due to either naturally occurring materials like halite that has not been washed out or deposits from the drilling process.

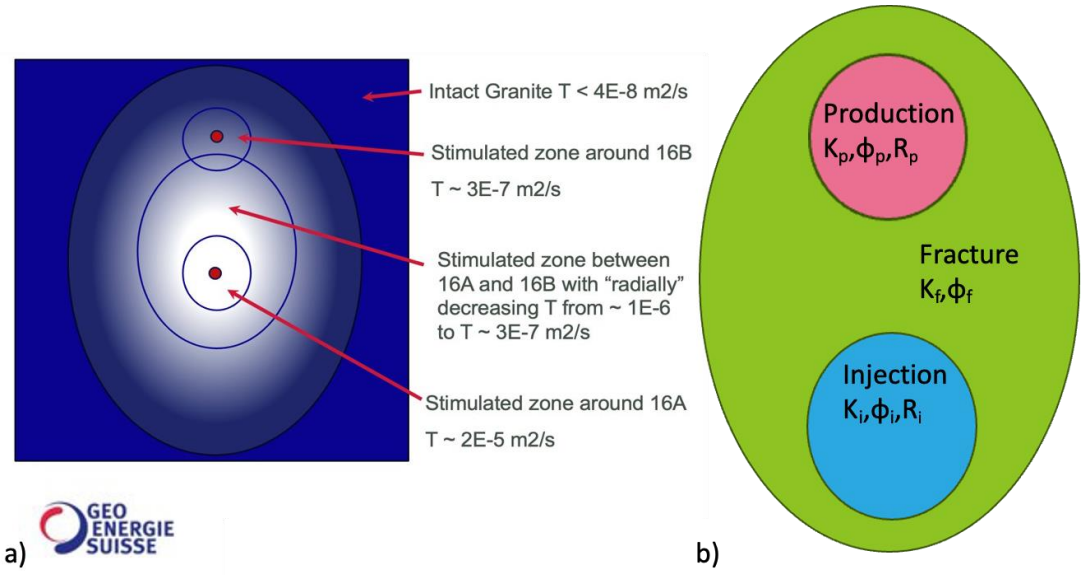

Figure 1: (a) Simplified conceptual model developed by Geo Energie Suisse fit to June 2023 slug testing in well 16A (Peter Meier, October 2023, internal meeting). (b) Conceptual model used in our simulations with three zones of permeability and porosity (injection, main fracture, production).

To better understand and characterize the fracture network and the regions of high and low transmissivity, the simulations in our work use a simplified model containing the three regions shown in Figure 1b. In the simulations that follow, we vary the permeability, porosity and radius (K,phi,R) of the three zones. These simulations include the four different characterizations of the fracture shown in Figure 2 and described in the caption.

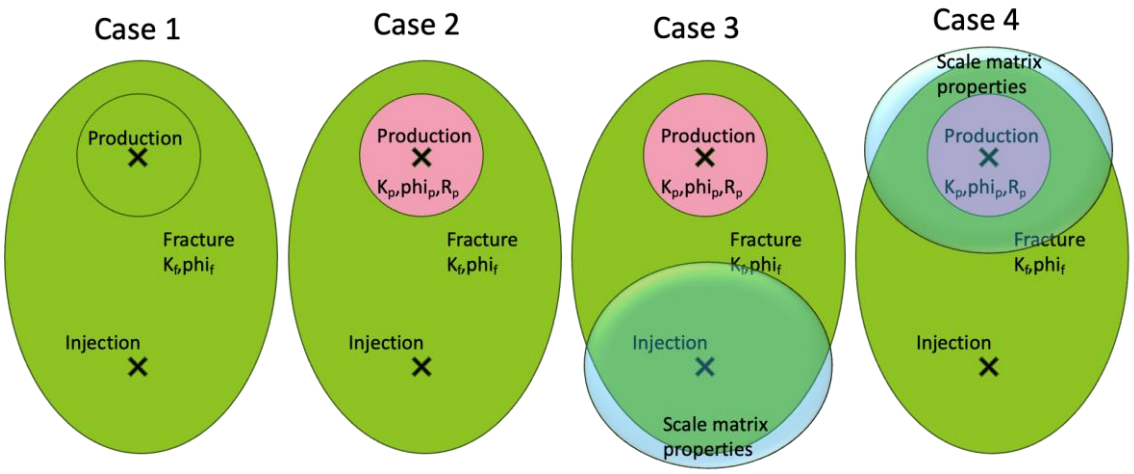

Figure 2: Four fracture characterizations simulated in this work. Case 1 uses a single set of properties for all regions of the fracture network. Case 2 has a single set of properties for the injection region and fracture regions with a lowered permeability around the production zone. Case 3 is similar to case 2 with an additional region of higher permeability extending into the matrix around the production well. Case 4 is similar to case 2 with an additional region of higher permeability extending into the matrix around the injection well. The production region has R_p=10 meters and the matrix scaled region has R=100 meters.

2. CIRCULATION TEST DATA

Two sets of circulation tests were performed in July 2023 to test connectivity between wells 16A and 16B. A comprehensive analysis of the circulation tests is given by Xing et. al. (2024). In this work we use pressure and mass data from the second set of circulation tests performed on July 18 and 19 to fit our THM model. Wellhead pressure, injection rate, and producing rate for the July 18 and 19 tests are given in Figure 3. The injection rates range from 2.5 to 7.5 bpm with a maximum pressure of 4500 psi during the July 18 circulation test. Injection well 16A contains three frac stages spaced approximately 300 feet apart where the bottom stage 1 is 200 ft of open hole at a depth of 10938 ft and stages 2 and 3 are cased and perforated. The flow rate for the July 18 and 19 The flow is partitioned between the three stages and the open hole stage 1 zone receives approximately 50% of the flow for the July 19 tests (Xing et al, 2023).

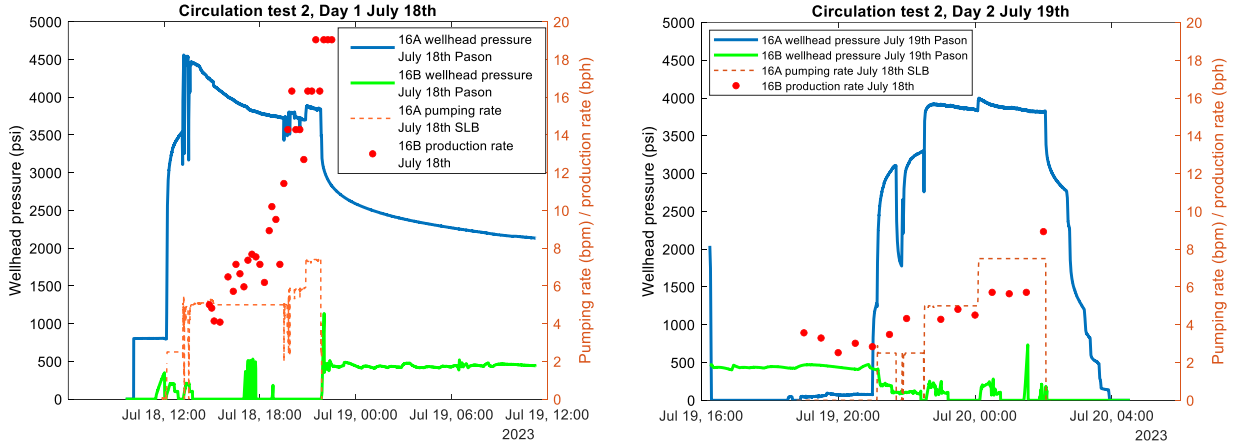

(a) *(b)*

Figure 2: Circulation test 2 data showing wellhead pressure, injection rate, and producing rate for (a) July 18 and (b) July 19, 2023 (after Figure 5 in Xing et al. 2024).

2. SIMULATION SET-UP AND RESULTS

Numerical models have been used to evaluate several of the 15 Key Points discussed above. The primary items being evaluated as part of this paper are treating the fractures in the reservoir as simple "penny shaped cracks" instead of a discrete fracture network, using spatially varying and/or zonated initial permeability in the fractures, and accounting for significant and time varying fluid storage in the intact reservoir surrounding the fractures. Four cases of zonated permeabilities are considered in this work, shown in Figure 2.

The circulation tests are modeled using fully coupled thermal-hydrological-mechanical finite element simulations using FALCON. Only the open toe at the bottom of well 16A is modeled (stage 1) using the domain shown in Figure 4a. The domain has dimensions 300m x 500m x 600m with symmetry boundary conditions placed between stages 1 and 2 (in the direction of the injection wells in Figure a). Half symmetry boundary conditions are also placed on the positive y-face where only half the fracture is modeled. The injected mass is divided in half to account for the half symmetry plane. Figure 3 also shows the discrete fracture network in green fit to the seismic cloud data (Finnila et al. 2023). Our model uses a single fracture shown by the white ellipse in Figure 4a to connect wells 16A and 16B with an area approximately equal the largest fracture in the seismic cloud DFN found near stage 3. The domain was meshed with a contiguous tetrahedral mesh shown in Figure 4b where the fracture is meshed with 2m elements that scale out to 20m at the boundary.

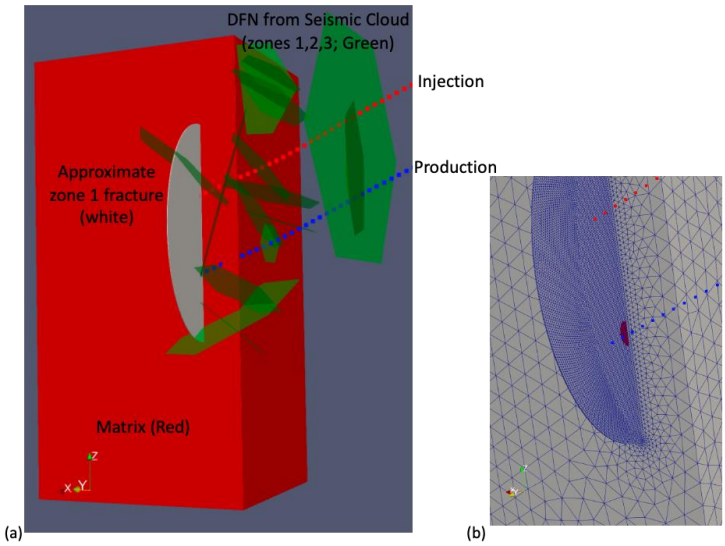

Figure 4: Thermo-Hydraulic-Mechanic simulation setup. (a) The matrix is shown in red with the fracture being modeled shown in white. The cold-water injection well 16A is shown by the blue dots and the hot-water production well 16B is show by the red dots. The discrete fracture network created by Finnila et al. 2023 fit to the seismic cloud data is shown in green. (b) Close up of the mesh used to represent the fracture (2m elements) and matrix (20m elements). The red region is where fluid is injected. Symmetry conditions are applied to the positive y and negative x faces.

Homogenized permeability and porosity fields were created by Finnila et al. 2021 based on the open hole log of 16A and 16B and seismic cloud data from the stimulation. The homogenized properties are given on a 10-meter mesh and are separated into those due to fractures and the background field. In this work we only use the background fields shown in Figure 3 as the purpose of this work is to characterize the fracture material properties on the 1m mesh shown in Figure 4b to reproduce the 16A wellhead pressure and 16B mass outflow shown in Figure 3. The background porosity and permeability fields are linearly interpolated onto the unstructured tetrahedral mesh with varying element sizes. In the far-field, the 20m tetrahedral elements contain the same volume as the 10m cubes used produce the homogenized fields.

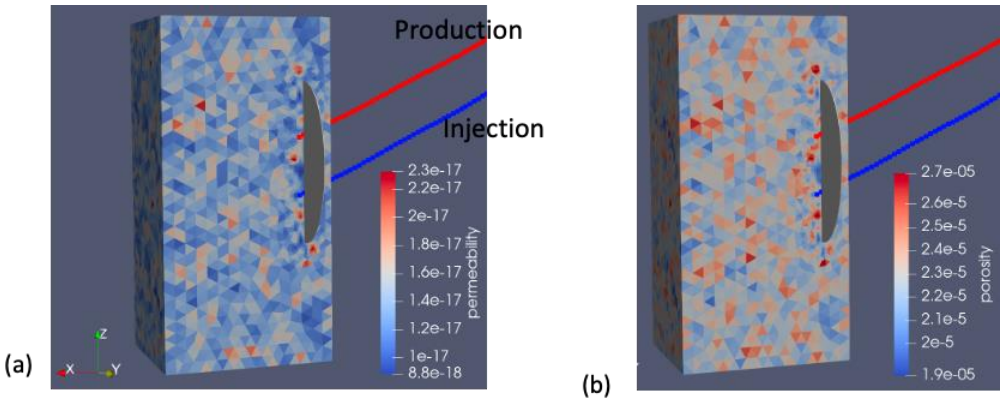

Figure 3: Homogenized background (a) permeability and (b) porosity fields (Finilia et al 2023?) linearly interpolated onto the tetrahedral mesh shown in Figure 4b.

2.1 Stochastic Thermal-Hydrological Modeling

For the simulations in this section, the four zonated fracture and porosity fields shown in Figure 2 are sampled over the range of properties given in Table 2 with results for injection well 16A relative pressure and production well 16B flow rates given in Figures 4-9. 60 parameter samples are taken for each case given in Table 2. The results given in this section use the July 18 injection schedule. The hydrological physics are modeled with Darcy flow and heat transfer is modeled within the advected porous fluid and the transfer of heat between the cold fluid to the hot matrix. The simplified physics and material models used in these simulations should approximate the porous flow in the fracture for the early time injection rate of 2.5 barrels per minute but cannot match the nonlinearities observed in the pressure histories when the injection rate is increased to 7.5 barrels per minute.

Table 2. Material property ranges for cases 1-4 shown in Figure 2. Fracture permeability (k) and porosity (φ) are sampled on logarithmic scale. Matrix scaling parameters are sampled on linear scale. 60 samples were taken for each case.

Case	k frac (m^2)	φ frac	k prod (m^2)	φ prod	k scale matrix	φ scale matrix
1	1e-14 to 1e-12	1e-3 to 1e-2	--	--	--	--
2	1e-14 to 1e-12	1e-3 to 1e-2	1e-16 to 1e-14	1e-4 to 1e-3	--	--
3	1e-14 to 5e-14	1e-3 to 1e-2	1e-16 to 1e-15	1e-4 to 1e-3	1 to 100	1 to 10
4	1e-14 to 5e-14	1e-3 to 1e-2	1e-16 to 1e-15	1e-4 to 1e-3	1 to 100	1 to 10

Figure 4 shows the simulation results for Case 1 where there is a single fracture region where parameters are sampled from a large range of values. Simulation results are colored by the fracture permeability or porosity. The best match to relative pressure comes from a fracture permeability of ~2.75 e-14 m^{-2}. The porosity controls the storativity of the fracture reflected by the slope of the relative pressure curve and using ϕ=3.3e-3 produces the closest fit. A single set of parameters can fit the relative pressure results, but the simulated production rate is 60x the measured field production results, i.e. the simulations show all the injected fluid reaching the production well, and at least a second zone of fracture parameters are needed to match the reduced field production rates.

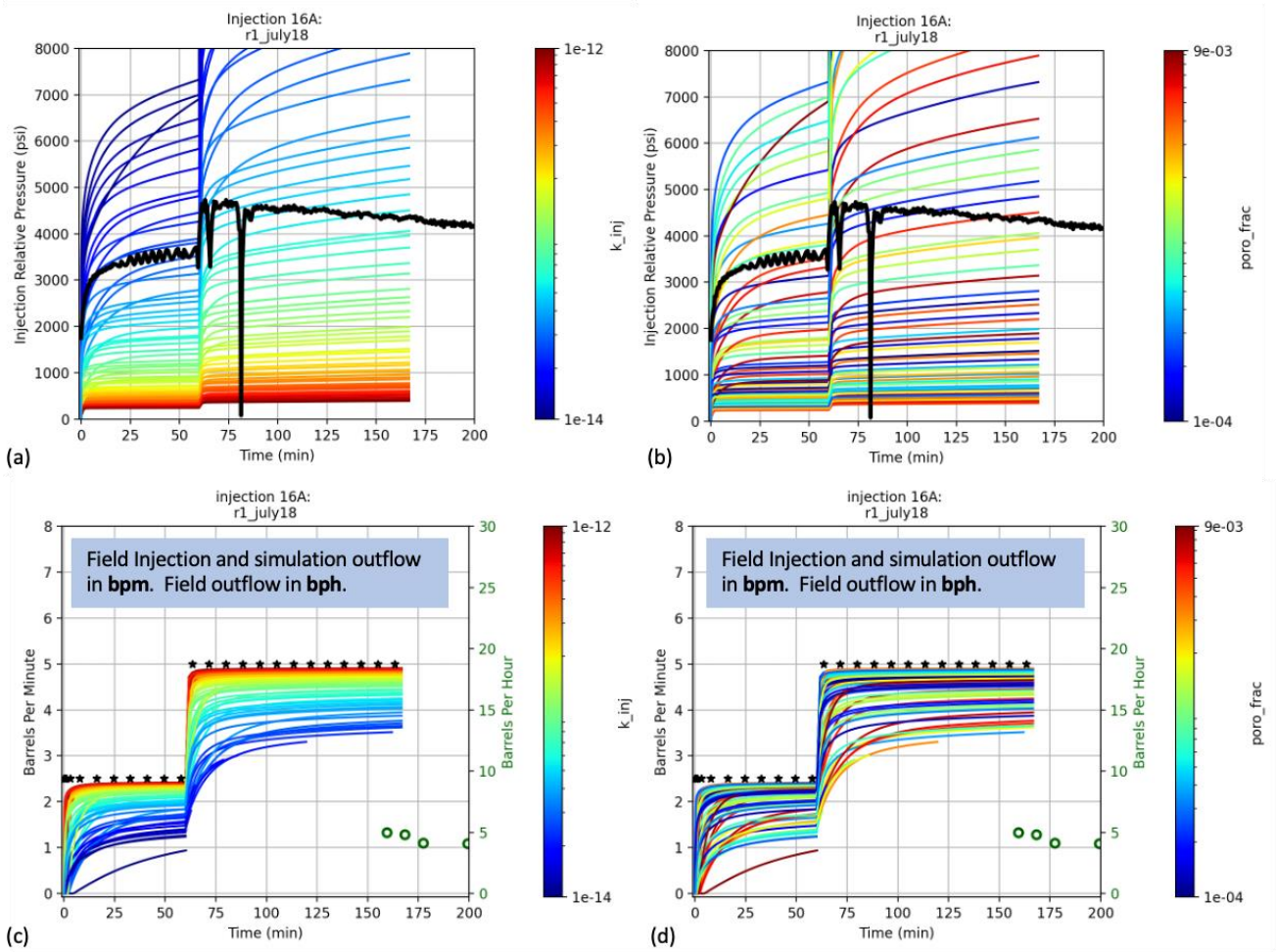

Figure 4: Case 1 sampling results: Top row is injection well relative pressure with field mesured values given by the black line and simulation results colored by (a) fracture permeability and (b) fracture porosity. The bottom row is the production flow rate where the field injection (black "*") and simulation production rate (colored lines) are in barrels per minute given on the left axis and the field production rate (green "o") is barrels per hour given on the right axis. The simulation production rates are colored by (c) fracture permeability and (d) fracture porosity.

The next set of simulations for Case 2 are shown in Figures 5 and 6. Case 2 contains two zones, a main fracture zone and a 10 meter zone around the production well where the permeability and porosity will be reduced in order to reduce the outflow where the simulated and field results are closer in Figure 6 and both are plotted in barrels per hour. The reduction in outflow leads to an increased relative pressure at the injection well 16A. This is especially true for simulated fractures with higher permeabilities near 1e-12m^{-2} which now produce about 2000 psi relative pressure. The relative pressure is closely correlated to the fracture permeability shown in Figure 5(a) and the production well mass production is most closely correlated to the production well permeability.

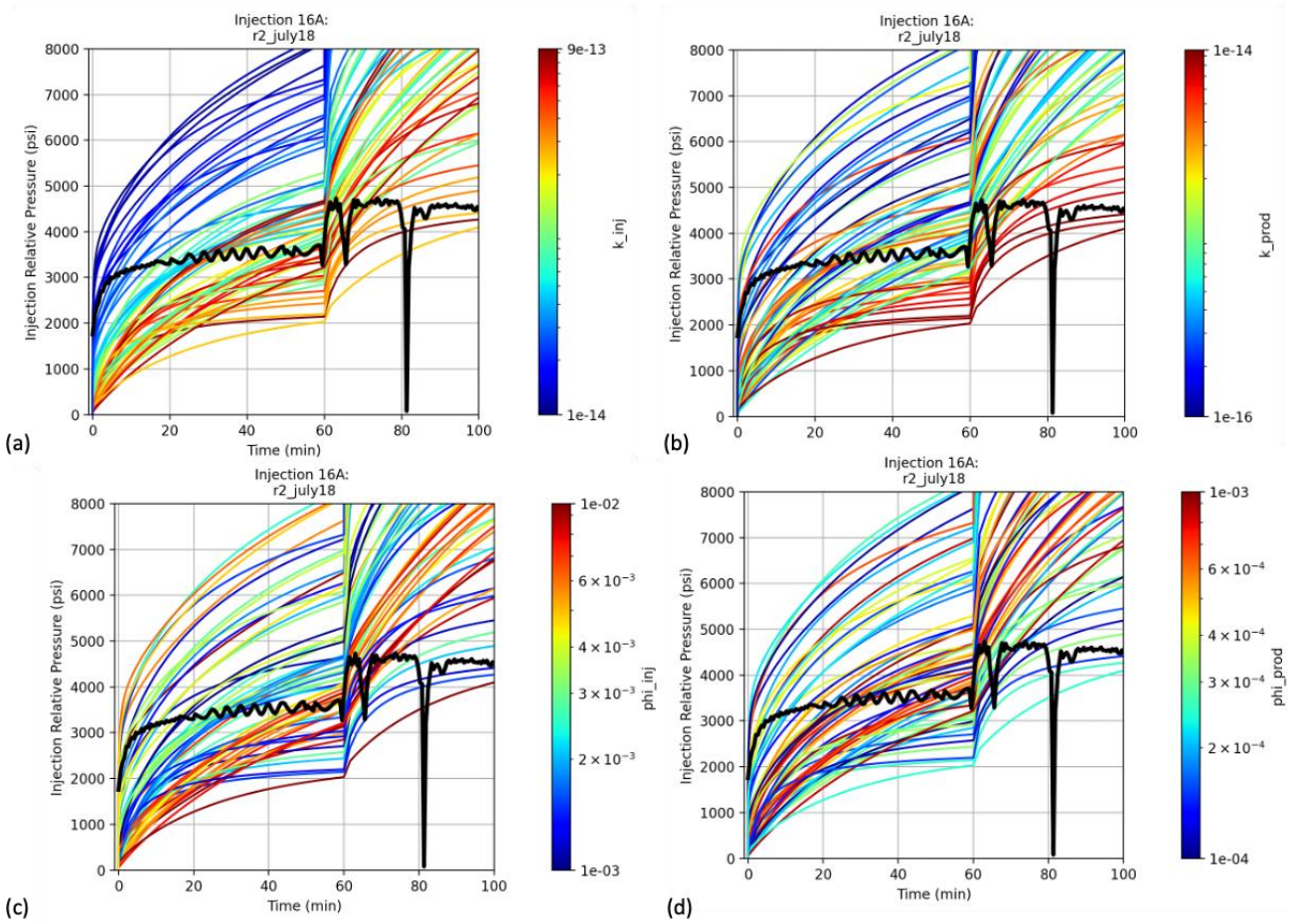

Figure 5: Case 2 sampling results for injection well relative pressure with field measured values given by the black line and simulation results colored by (a) fracture permeability, (b) production well permeability, (c) fracture porosity, and (d) production well porosity.

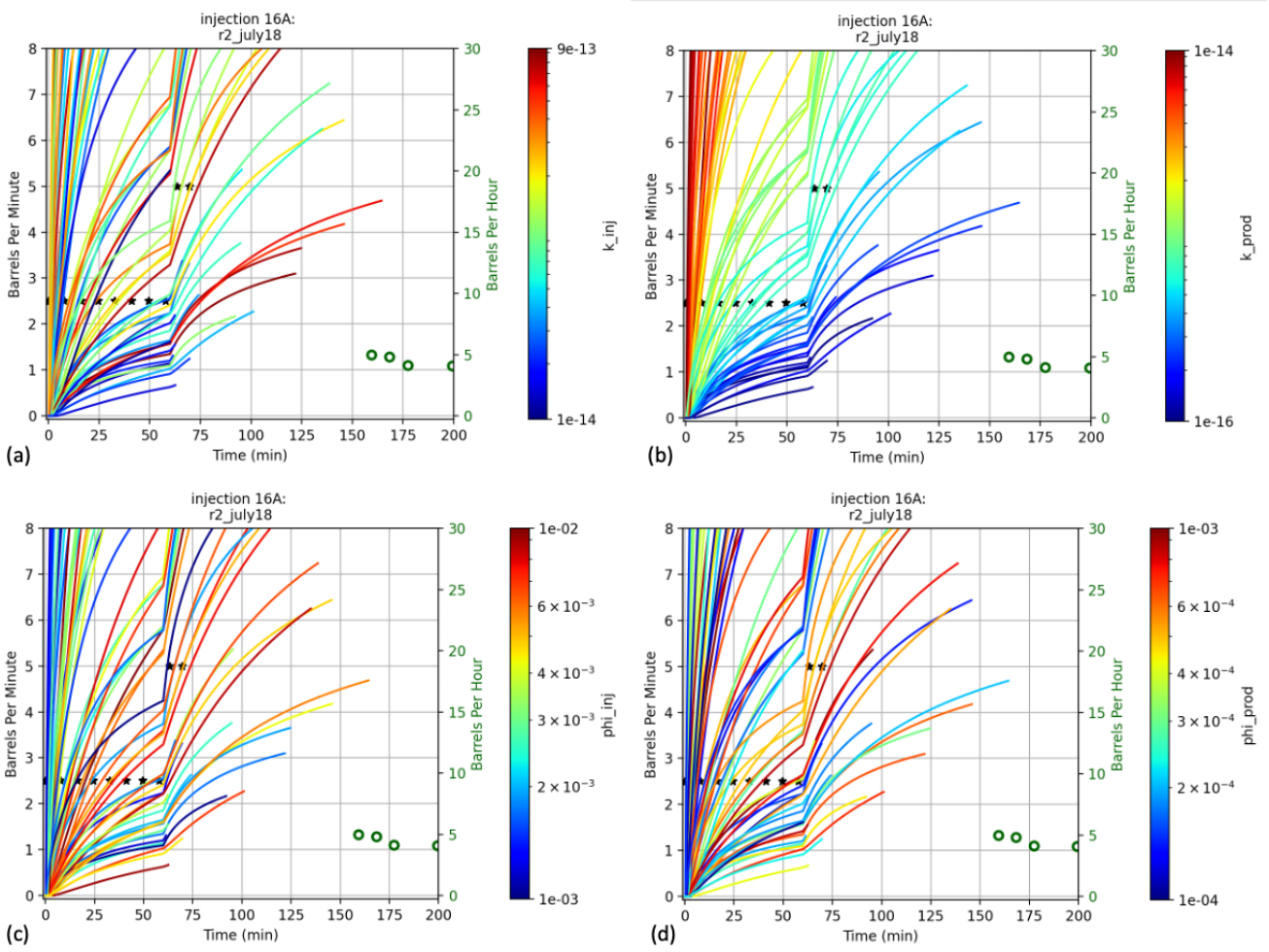

Figure 6: Case 2 sampling results for production rate colored by (a) fracture permeability, (b) production well permeability, (c) fracture porosity, and (d) production well porosity. The field injection rate (black "*") is measured in barrels per minute on the left axis and the production rates for the both the simulation (colored lines) and field measurement (green "o") are in barrels per hour.

Simulation results for Case 3 are shown in Figures 7 and 8 where the matrix properties within 100 meter radius around injection well 16A are scaled. The large increase in injection well pressure due to the increased permeability around the production well 16B modeled in Case 2 indicated that the fluid being injected needs to be taken in by a larger volume than that available by the fracture. The matrix properties shown in Figure 3 are sampled over a range of values (1-100x for permeability and 1-10x for porosity). The ranges for the fracture and production zone permeabilities are also reduced based on the results from Cases 1 and 2. For this set of simulations, the relative pressure change in well 16A appears to be equally influenced by the fracture permeability and matrix permeability scaling. The outflow shown in Figure 8 is still closely correlated to the production well 16B permeability.

For Case 4, the matrix scaling is centered around the production well 16B. The relative pressure and production rates for Case 4 are shown in Figure 7. These results are like Case 2 where the relative pressure is closely correlated to the fracture permeability and the production rate from 16B is closely correlated to with the lower permeability zone around 16B. In the next section, we attempt to fit the pressure change and production rate for the pumping schedules used on July 18 and 19 by choosing material properties based on the trends observed in this section. Cases 3 and 4 suggest that the matrix should be scaled around the injection well 16A. The slopes of the pressure curves for Cases 2-4 also suggest that a constant scaling is probably not correct and that the scaling should decrease exponentially as was used by Geo Energie Suisse their analysis.

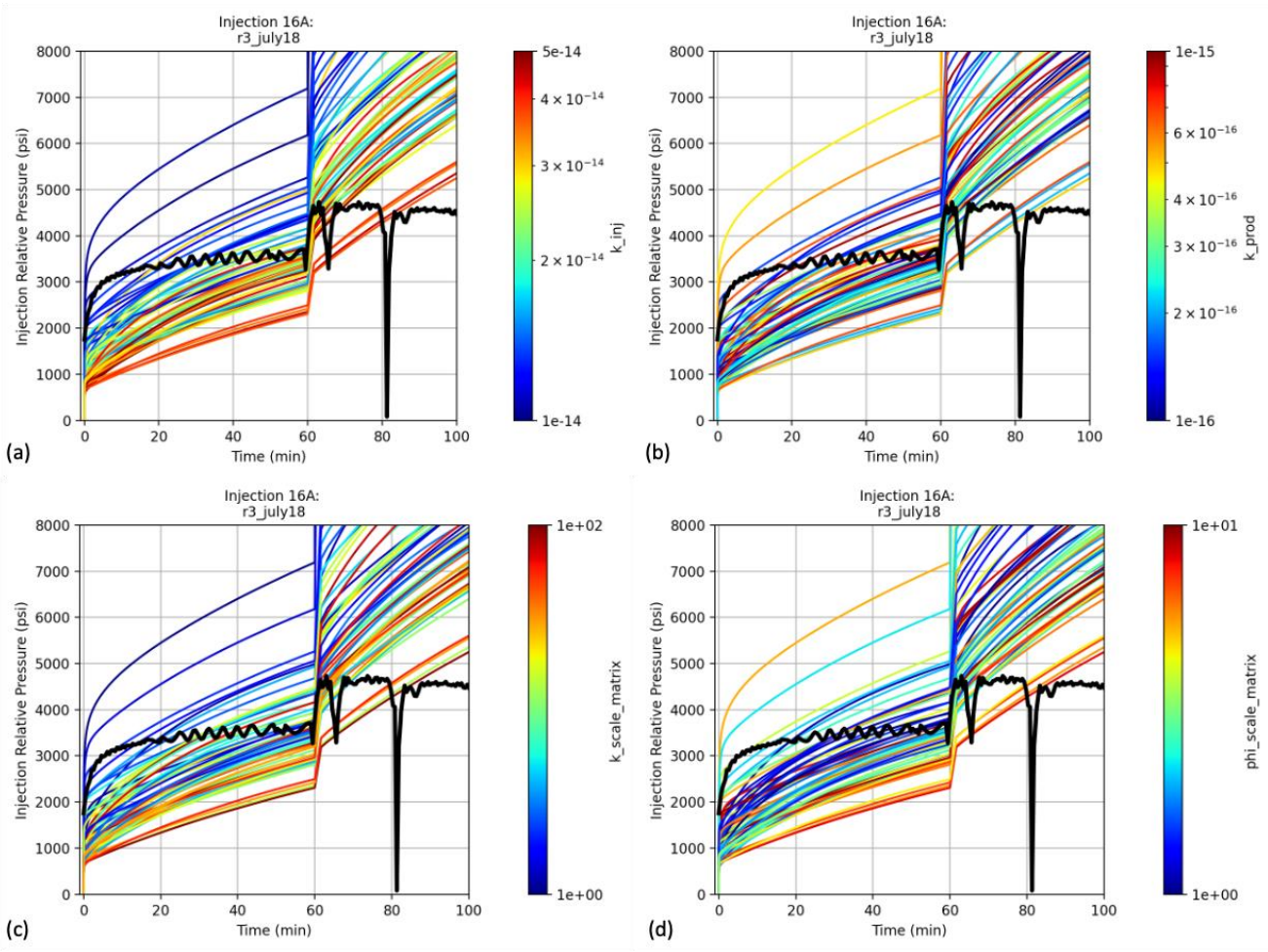

Figure 7: Case 3 sampling results for injection well relative pressure with field measured values given by the black line and simulation results colored by (a) fracture permeability, (b) production well permeability, (c) matrix permeability scale factor, and (d) matrix porosity scale factor.

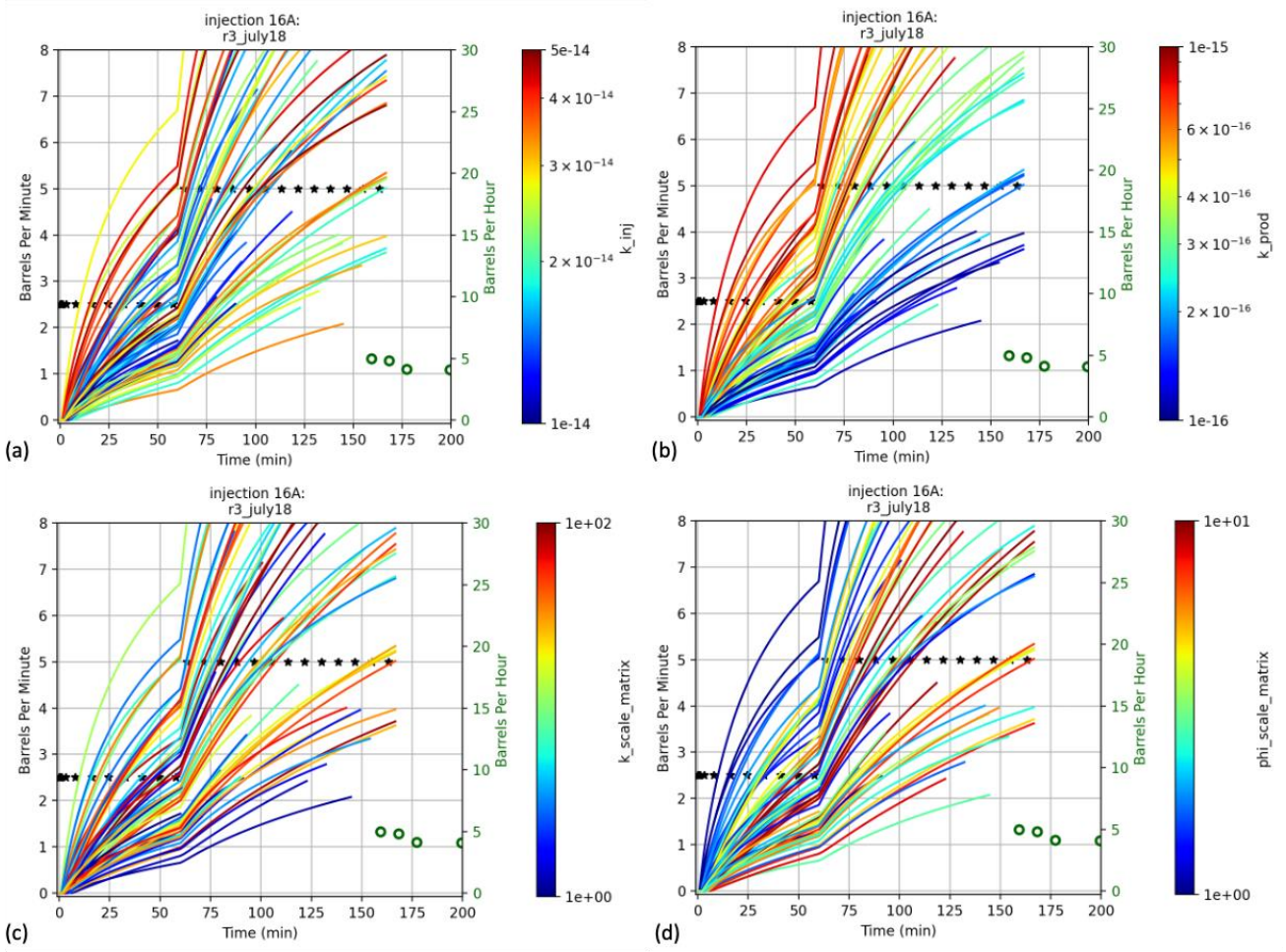

Figure 8: Case 3 sampling results for production rate colored by (a) fracture permeability, (b) production well permeability, (c) matrix permeability scale factor, and (d) matrix porosity scale factor. The field injection rate (black "*") is measured in barrels per minute on the left axis and the production rates for the both the simulation (colored lines) and field measurement (green "o") are in barrels per hour.

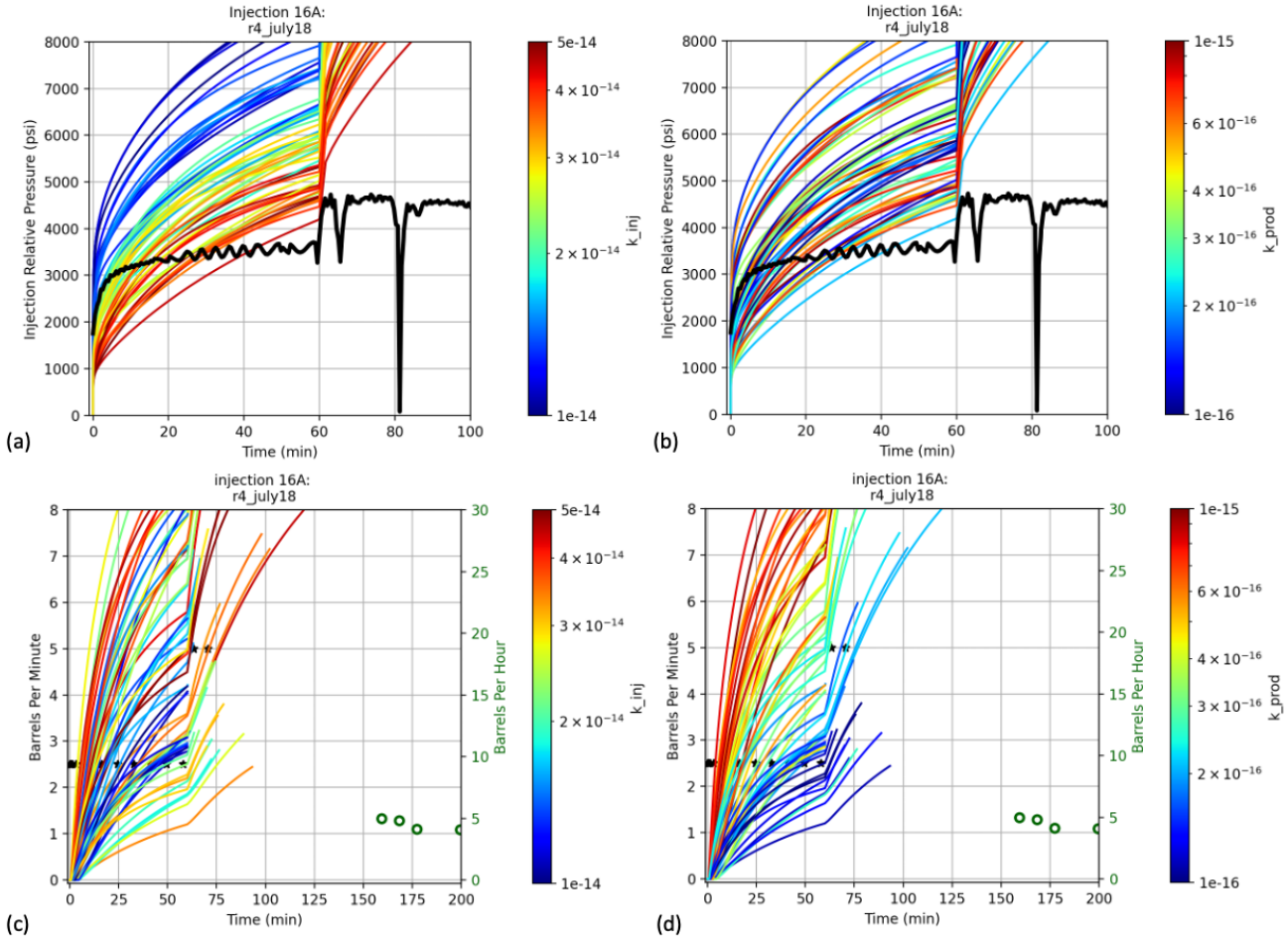

Figure 9: Case 4 sampling results: Top row is injection well relative pressure with field mesured values given by the black line and simulation results colored by (a) fracture permeability and (b) production well permeability. The bottom row is the production flow rate where the field injection rate (black "*") is in barrels per minute given on the left axis and the simulation (colored lines) and field production (green "o") rates are barrels per hour given on the right axis. The simulation production rates are colored by (c) fracture permeability and (d) production well permeability.

2.2 Best Fit Thermal-Hydrological Modeling

In this set of simulations, the fracture and porosity fields are fit to the early time 16A wellhead pressure and 16B production rate for the July 18 and 19 circulation tests where the injection rate is only 2.5 barrels per minute. These simplified physics cannot match the nonlinearities observed in the pressure histories when the injection rate is increased to 7.5 barrels per minute. The hydrological physics are modeled with Darcy flow and heat transfer is modeled within the advected porous fluid and the transfer of heat between the cold fluid to the hot matrix. The main effect of the thermal physics is through the water equation of state.

The porous flow properties are held constant in these simulations, i.e. they are not a function of pore pressure. In the first set of simulations shown by the solid and dashed red lines in Figure 10, the matrix permeability and porosity fields shown in Figure 3 are used with spatially constant fracture properties of k=2.75 e-14 m^{-2} and ϕ=3.3e-3. The simulated early time well head pressure (solid red line) is closely matched with the field data (black line) however all the injected fluid in the simulation reaches the production well (dashed red line). The production field results show only 1/60 of the injected water (* measured in bpm) reaching the production well (**o** measured in bph).

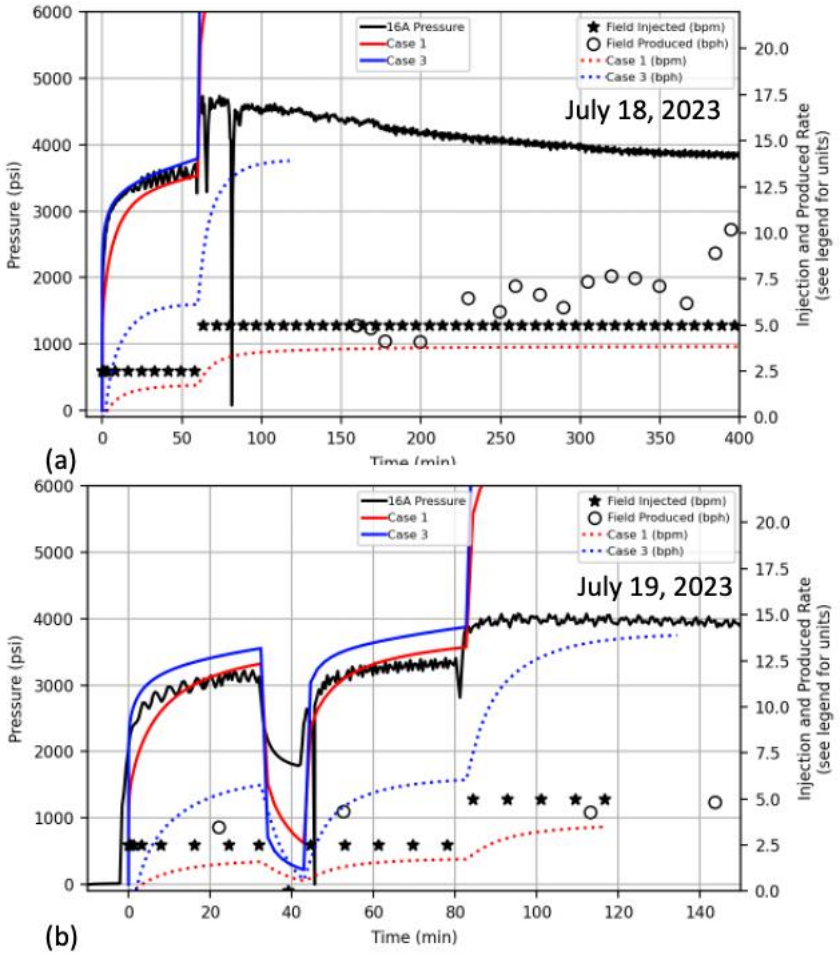

Figure 10: Experimental field data (black data) and simulation results (colored data) for the (a) July 18 and (b) July 19, 2023 circulation test. The left axis and solid lines show pressure data where both simulations match the early time field data. The dashed lines and markers show injection and production data. Note the units of the constant property dashed line in blue is in barrels per minute (bpm) and the spatially varying properties are in barrels per hour (bph).

The next set of simulations use a spatially varying permeability and porosity fields shown in Figure 11 to reduce the outflow in well 16B while maintaining the injection pressure. The fracture properties have a constant porosity with an exponential reduction in permeability between the injection and production well to reduce the production rate to match the early time experimental data. The permeability is held constant within 50 meter of the injection well. A close match to the early time pressure is obtained by exponentially scaling the matrix permeability and porosity as a function of distance from the injection point. The matrix properties are scaled over a 100m radius. Outside the scaling region the matrix permeability is scaled by 10x. The reduction in outflow causes these simulations to go beyond the pressure bounds (>100MPa) of the water equation of state when the injection rate is increased to 7.5 barrels per minute. An analysis on well 16A slug and low flow rate connectivity tests by Geo Energie Suisse and presented by Podgorney 2024, used a similar exponentially varying transmissivity.

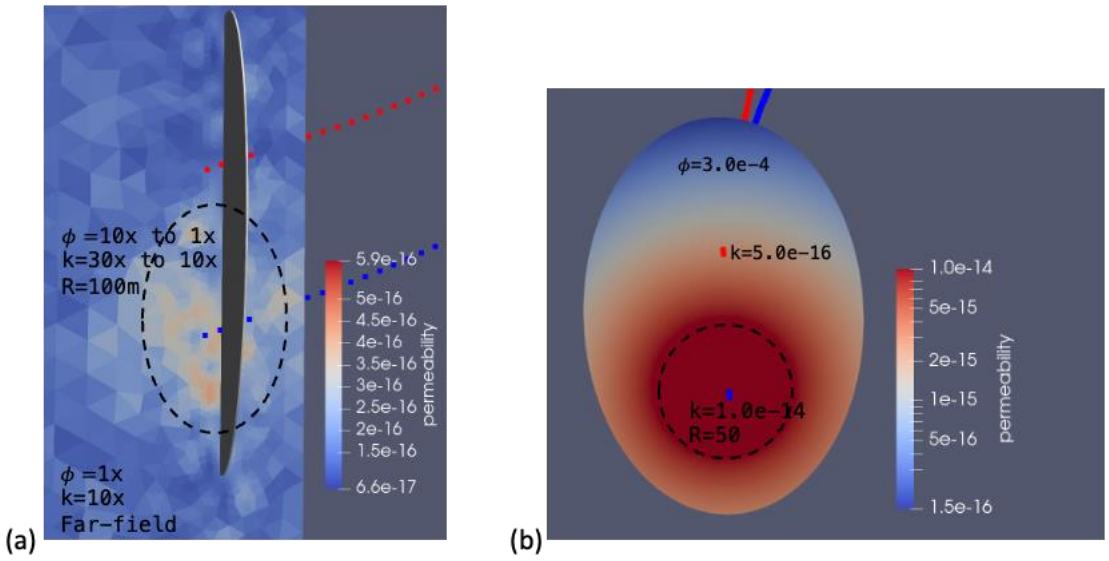

Figure 11: Experimental field data (black data) and simulation results (colored data) for the July 18, 2023 circulation test. The left axis and solid lines show pressure data where both simulations match the early time field data.

2.3 Thermal-Hydro-Mechanical Modeling

The next set of simulations are a work in progress and will be updated in the electronic version of this paper available online. They attempt to match the later stages of the circulation test where pore pressure in the aperture will cause it to open leading to an increase in permeability and porosity. This coupling is accounted for by scaling the permeability and porosity by the volumetric strain. Even with this coupling, we are unlikely to match the pressure response which is likely due to extension of the fracture network which is not currently being accounted for in our models. A preliminary set of results are shown in Figure 12 where only the linear scaling factor between the permeability and volumetric strain is varied over 3 orders of magnitude. None of the pressure responses show the pressure drop observed in the field data which is likely due to fracture growth. The produced rate shown by the dashed lines closely matches the field data shown by the open circles.

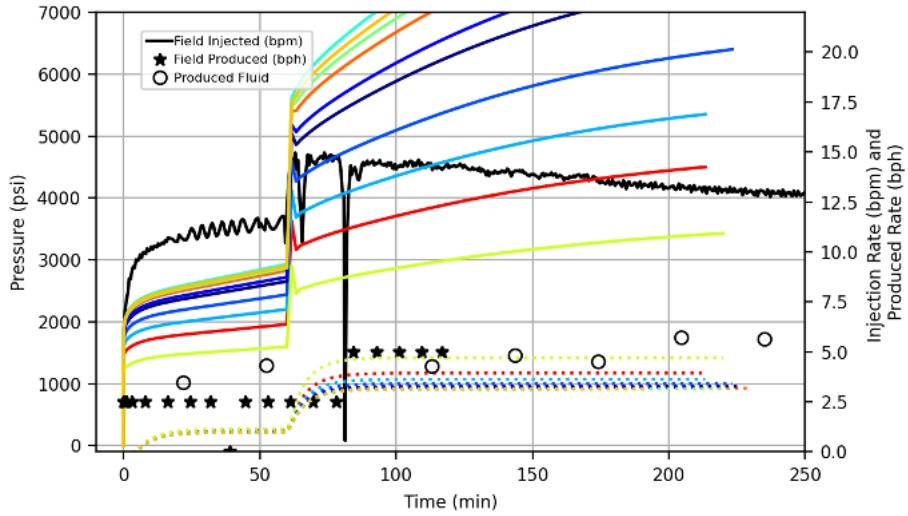

Figure 12: Experimental field data (black data) and THM simulation results (colored data) for the July 18, 2023 circulation test. The left axis and solid lines show pressure data where both simulations match the early time field data. The solid simulations lines are relative pressure and the dotted lines are produced rate in bph.

3. CONCLUSIONS

Reevaluation of the original FORGE numerical models was undertaken based on based on a review of the July circulation tests. In this work we numerically tested several of the conceptual models to evaluate the fracture properties. Key findings from the low flow rate

injections are that there is a large, highly permeable fracture network surrounding the injection zone with most of the fluid flowing into fractures that are weakly connected to the production well. This zone is represented in our models using spatially varying permeability and porosity. To match both the well head pressure and outflow rate, the matrix porous flow properties had to be increased by about 10x that of the background matrix material properties. Future work will explore better methods for coupling mechanics and porous flow and the extension of the fracture network under these conditions.

ACKNOWLEDGEMENTS

Funding for this work was provided by the U.S. DOE under grant DE-EE0007080 "Enhanced Geothermal System Concept Testing and Development at the Milford City, Utah FORGE Site." We thank the many stakeholders who are supporting this project, including Smithfield, Utah School and Institutional Trust Lands Administration, and Beaver County, as well as the Utah Governor's Office of Energy Development.

This research made use of the resources of the High Performance Computing Center at Idaho National Laboratory, which is supported by the Office of Nuclear Energy of the U.S. Department of Energy and the Nuclear Science User Facilities under Contract No. DE-AC07-05ID14517.

REFERENCES

Finnila, A., Damjanac, B. and Podgorney, R. 2023. Development of a Discrete Fracture Network Model for Utah FORGE using Microseismic Data Collected During Stimulation of Well 16A(78)-32. In proceedings, 48th Workshop on Geothermal Reservoir Engineering, Stanford University, Stanford, California, February 6-8, 2023, SGP-TR-224.

Pengju X., England, K., Moore, J., Podgorney, R. and McLennan, J., 2024, January. Analysis of Circulation Tests and Well Connections at Utah FORGE. In proceedings, 49th Workshop on Geothermal Reservoir Engineering, Stanford University, Stanford, California, February 12-14, 2024, SGP-TR-227.

Pengju X., Damjanac, B., Radakovic-Guzina, Z., Torres, M., Finnila, A., Podgorney, R., Moore, J., and McLennan, J., 2023, Comparison of Modeling Results with Data Recorded During Field Stimulations at Utah FORGE Site. In proceedings, 48th Workshop on Geothermal Reservoir Engineering, Stanford University, Stanford, California, February 6-8, 2023, SGP-TR-224.

Finnila, A., Doe, T., Podgorney, R., Damjanac, B., and Xing, P., 2021, Revisions to the Discrete Fracture Network Model at Utah FORGE Site, GRC Transactions, Vol. 45, (2021).

Podgorney, R., 2024, Utah FORGE Modeling and Simulation Community Forum: Overview of October 2023 Data Review and Conceptual Model Update Meeting (https://utahforge.com/numerical-modeling/#m-s-forum). (November 2024)